Temperature dependence green reduction of graphene oxide by urea

Pankaj Chamoli[1], Malay K. Das[2], Kamal K. Kar[1, 2*]

[1]*Advanced Nanoengineering Materials Laboratory, Materials Science Programme, Indian Institute of Technology Kanpur, Kanpur, India*
[2]*Advanced Nanoengineering Materials Laboratory, Department of Mechanical Engineering, Indian Institute of Technology Kanpur, Kanpur, India*

[*]Corresponding author, Tel: (+91) 512-2597687; Fax: (+91) 512-2597408; Email: kamalkk@iitk.ac.in

Received: 20 March 2016, Revised: 11 August 2016 and Accepted: 22 November 2016

DOI: 10.5185/amlett.2017.6559
www.vbripress.com/aml

Abstract

In the present study, temperature dependence reduction of graphene oxide into graphene nanosheets has been demonstrated using green reducing agent, urea. As synthesized graphene nanosheets have been characterized by Raman spectroscopy, Fourier transform infrared spectroscopy (FTIR), UV-visible spectroscopy(UV-Vis), X-ray diffraction (XRD), field emission scanning electron microscopy (FESEM), and X-ray photon spectroscopy (XPS). Raman analysis confirms that the maximum reduction of graphene oxide is observed at 140 ºC, and reached to high Raman D to G band intensity ratio of ~ 1.41. FTIR analysis supports the Raman signature of maximum reduction of oxygen functional groups from graphene oxide at 140 ºC. XPS analysis validates the Raman and FTIR signature of maximum removal of oxygen species from graphene oxide at 140 ºC, and confirms the attainment of the C/O ratio of ~ 5.66. Result indicates that the urea offers excellent reductive ability at high temperature to produce graphene nanosheets. Copyright © 2017 VBRI Press.

Keywords: Graphene nanosheet, green reduction, graphene oxide, reducing agent, urea.

Introduction

The youngest member of the carbon nanostructured family, graphene, a flat monolayer of sp^2 hybridized carbon atoms densely packed into hexagonal honeycomb structure, has received great attention in the scientific community worldwide due to its remarkable properties including high room temperature mobility of charge carriers (~ 2 x10^5 cm^2 V^{-1} s^{-1}), optical absorption ($\pi\alpha$) ≈ 2.3%, where α is the fine structure constant), high optical transparency (~ 97.7%), Young's modulus (~1 TPa), excellent intrinsic strength (~130 GPa), exceptionally high thermal conductivity (~5000 W m^{-1} K^{-1}), and enormous specific surface area (2620 m^2 g^{-1}); and called as a "miracle material" **[1]**. These extraordinary and intriguing properties open its potential applications in verity of areas such as nanoelectronics, electrochemical, energy storage, carbon dioxide (CO_2) adsorption, flexible touch panels, and thin film photovoltaic **[2-6]**; and wide variety of biomedical applications including biosensors, drug delivery, tissue engineering and bio-imaging, which increases the concrete demand for cost-effective and environmentally friendly methods for mass production of graphene [**7**, **8]**. As an evidence, European commission has announced €1 billion funding to the graphene research and its commercialisation for over the next ten years **[9]**.

To date, the most common and versatile way for the large scale production of graphene is based on oxidation of graphite and exfoliation followed by chemical reduction via solution-processable routes. This oxidative-exfoliation method produces graphene oxide (GO) at large scale having oxidized graphene-like nanosheets, which require additional treatment of reduction to produce graphene nanosheets. For reduction process of GO researchers have reported various reducing agents such as hydrazine or dimethylhydrazine, hydroquinone and sodium borohydride etc. Such reducing agents have toxic/corrosive nature and very harmful to our environment. As an alternative, less toxic reducing agents including sodium hypophosphite (Na_3PO_2) [**10**], sulfuric acid (H_2SO_4) [**11**], aluminium iodide (AlI_3) [**12**], bismuth ferrite ($BiFeO_3$) [**13**] and metal nanoparticles [**14**] etc., have been explored to reduce GO. But, some amount of harmful chemical traces has been found on the graphene surface by these reducing agents during reduction. As a result the produced graphene is not suitable for bio-related applications **[15]**. As the consequence, green methodologies have been investigated to reduce GO into graphene nanosheets such as green tea [**16**], vitamin C [**17**], glucose [**18**], sugar [**19**], melatonin [**20**], bovine serum albumin[**21**], ginseng [**22**], bacteria [**23**], curcumin [**24**], bacteriorhodopsin [**25**], cow urine [**26**] etc., to minimize the negative environmental impacts as well as suitability for biomedical applications. In addition, urea has been used as a green reducing agent for reduction of GO to produce reduced graphene oxide (rGO) and low

temperature reduction has also been reported by different groups. For example, time dependant study at 95 ^{o}C has been carried out by Lei *et al*. via facile solution-processable approach for reduction of GO to produce stable rGO [**27**]. Yang *et al*. have fabricated rGO based novel gas sensor, using urea as a green reducing agent for GO at 100 ^{o}C [**28**]. Notably, during reduction process the structural transformation takes place i.e., sp^3 C-O bonds to sp^2 hybridized C-C bonds of GO with temperature, which leads to better electronic properties of graphene nanosheets [**29**]. Hence, temperature is an important factor during reduction of GO.

Till now, temperature-dependent systematic study on the reductive ability of urea has not been reported. The main objective of present study is to establish the temperature-dependant reduction of GO using green reducing agent, urea. The reductive ability of urea has been tested over a range of temperature i.e., 27 to 140 ^{o}C. Experimental results confirm that the maximum removal of oxygen functionalities is observed from GO at 140 ^{o}C. This study is noteworthy due to the eco-friendly nature of urea towards the bulk scale production of graphene nanosheets.

Experimental

Materials

Graphite (natural graphite powder, purity ≥ 99.9%) was obtained from Loba Chemie Pvt. Ltd., Mumbai, India and used as carbon source. In addition, sodium nitrate ($NaNO_3$, purity ≥ 98%), sulfuric acid (H_2SO_4, 98%; purity ≥ 99%), potassium permanganate ($KMnO_4$, purity ≥ 99%), hydrogen peroxide (H_2O_2, 30%; purity ≥ 99.7%) and urea (CH_4N_2O, purity ≥ 99.5%) were received from Qualigens Fine Chemicals, Mumbai, India. All materials were analytic grade and used without further purification.

Methods

Preparation of GO

GO was prepared by modified Hummer's method as reported elsewhere **[26]**. Briefly, H_2SO_4 (140 mL) and $NaNO_3$ (2.5 g) were mixed with graphite powder (5 g) under ice bath. Then, $KMnO_4$ (15 g) was mixed slowly in above mixture maintaining the temperature below 20 ^{o}C. After sifting the mixture into water bath (35 ^{o}C) and stirring for 0.5 h, the solution color is changed from green to purple brown paste. Deionized (DI) water (230 mL) was added slowly to the mixture and temperature was raised to 98 ^{o}C. Further, DI water (500 mL) and H_2O_2 (50 mL) were added slowly and stirred for 0.5 h. The yellowish color of mixture was appeared, which indicates the harsh oxidation of graphite powder. Finally, the solution was allowed to cool at room temperature, and the solution was filtered and washed several times with DI water for the removal of remaining solvent until pH ~7 reached. The resultant GO was dried at 60 ^{o}C for overnight in ambient condition.

Reduction of GO

Dried GO powder (10 mg) prepared by a modified Hummer's method was suspended in 100 mL DI water with strong stirring and ultrasonicated at 100 Watt for 2 h to form homogenous dispersion. Once, GO was fully dispersed in DI water than 2.5 g urea was mixed in the dispersion. Further, resultant solution was directly shifted into oil bath with continuous stirring at different temperatures 27, 60, 90, 120 and 140 ^{o}C for 24 h. Resultants were filtered with 0.2 micron membrane filter and washed several times with DI water and dried for 3 h in vacuum oven at 60 ^{o}C. The graphene nanosheets synthesized at temperatures of 27, 60, 90, 120 and 140 ^{o}C were named as UGns-1, UGns-2, UGns-3, UGns-4 and UGns-5, respectively.

Characterizations

Raman analysis

Raman spectra were collected by LabRam Micro-Raman spectrometer (Jobin-Yuon HR 800 UV with a He–Ne laser excitation source λ-633 nm). The spectrum was recorded in the spectral range of 700-3000 cm^{-1}.

Fourier transform infrared spectroscopy

Fourier transform infrared spectroscopy (FTIR) spectra were collected by Bruker-FTIR using KBr pallet. The spectrum was recorded in the spectral range of 4000–400 cm^{-1}.

UV–visible spectroscopy

UV–visible spectroscopy (UV-vis) were acquired by Perkin-Elmer Lambda 1050 with a UV-vis-NIR spectrophotometer. The spectrum was acquired in the wavelength range of 200–800 nm.

X-ray diffraction

X-ray diffraction (XRD) was studied by X'Pert Powder PANalytical using Advanced X-Ray Diffractometer with a Cu Kα adsorption spectrometer. The XRD pattern was collected in the scan range of 5–70^{o} (2 theta) with a scan step size of 0.0131.

Surface morphology

Surface morphology was taken by field scanning electron microscopy (FESEM) from JEOL JSM-7100F.

X-Ray photoelectron spectroscopy

X-Ray photoelectron spectroscopy (XPS) was used to test the surface compositional analysis by Multifunctional XPS ULVAC, PHI500 VersaProbe II with 1486.6eV Kα Al X-ray source. Data analysis was performed with XPSPEAK41 software using a Shirley background.

Results and discussion

Raman analysis

Raman spectroscopy is the most important tool to determine the different features of honeycomb network structure of carbon such as defect density, number of layers, doping, disorder, strain, types of edge, etc. Raman spectra of GO, UGns-1, UGns-2, UGns-3, UGns-4 and UGns-5 are shown in **Fig.1**. GO exhibits a prominent peak of pristine graphite at 1595 cm^{-1}, which corresponds

to G band and arises due to the E_{2g} phonon mode of sp^2-bonded carbon atoms; and disordered graphite peak at 1335 cm^{-1} corresponding to D band arises due to the unsatisfied Raman fundamental selection rule of zone-boundary phonons. Additionally, less intense peak at 2627 cm^{-1} corresponding to 2D band arises due to the second order zone boundary phonons as shown in **Fig. 1a** [**30**]. The ratio of relative intensity of the Raman D and G bands (I_D/I_G) gives an estimation of the disorder level in honeycomb structure, and generally exhibits a non-monotonic behaviour. The I_D/I_G ratio of ~1.10 is found for GO. During reduction process, new defects are introduced in the carbon skeleton, which create more elastic scattering, results an increase in the relative intensity ratio of Raman bands (I_D/I_G) [**30**]. Raman spectrum of UGns-1 shows D and G band at 1335 and 1598 cm^{-1}, respectively; and I_D/I_G ratio of ~1.11 is found. This indicates that the less amount of removal of oxygen species is observed at 27 °C from honeycomb network as shown in **Fig. 1b**. While, Raman spectrum of UGns-2 shows D band at 1337 cm^{-1}, G band at 1598 cm^{-1}, and I_D/I_G ratio of ~1.12. This clearly shows the more removal of oxygen species as shown in **Fig. 1c**. Raman spectrum of UGns-3 shows D band at 1339 cm^{-1}, G band at 1599 cm^{-1}, and I_D/I_G ratio of ~1.14; strongly suggests that more amount of removal of oxygen functional groups is observed from carbon skeleton as shown in **Fig. 1d**. Raman spectrum of UGns-4 shows D band at 1340 cm^{-1}, G band at 1602 cm^{-1}, and I_D/I_G ratio of ~1.20; signifies the high amount of removal of oxygen functional groups compared to UGns-1, UGns-2 and UGns-3 as shown in **Fig. 1e**. Moreover, Raman spectrum of UGns-5 shows maximum I_D/I_G ratio of ~1.41, strongly indicates the maximum reduction of oxygen functionalities at 140 °C from two dimensional honeycomb network as shown in **Fig. 1f**.

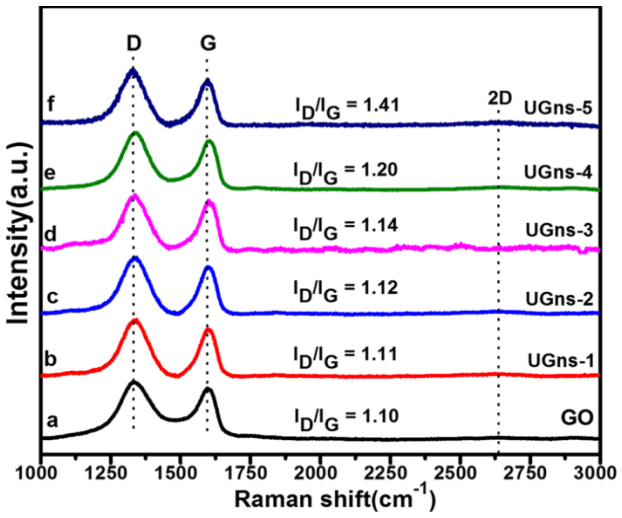

Fig. 1. Raman spectra of (a) GO, (b) UGns-1, (c) UGns-2, (d) UGns-3, (e) UGns-4 and (f) UGns-5.

In addition, D and G bands are red shifted to ~1340, 1602 cm^{-1} as compared to GO, also indicates that the π-conjugation is restored in sp^2-carbon network. The crystalline domain size (La) has been calculated by the Tuinstra−Koenig (TK) relation: La (nm) = $(2.4\times10^{-10})\times\lambda^4\times(I_D/I_G)^{-1}$, where λ ~ 633 nm; and found ~ 35.03 nm for GO, and 34.71, 34.40, 33.80, 32.11, 27.32 nm for UGns-1, UGns-2, UGns-3, UGns-4 and UGns-5, respectively. Decreased crystalline domain size suggests that the more disordered arrangement has been introduced in the honeycomb lattice during reduction process [**30**]. The reduction mechanism can be justified on the basis of high amount of nitrogenous compound present in urea, which accelerates redox reactions between electrochemically active functional groups (present in the carbon skeleton) and H_2O. This redox reaction promotes maximum reduction of GO at high temperature, leads the high yield graphene nanosheets [**31**].

Fourier transform infrared spectroscopy (FTIR)

FTIR spectroscopy is an important tool to study different functional groups present in carbon skeleton. **Fig. 2** shows the FTIR spectra of GO, UGns-1, UGns-2, UGns-3, UGns-4 and UGns-5. FTIR spectrum of GO shows broad peak at 3420 cm^{-1}, ascribes to hydroxyl groups (O-H) on 2D plane of honeycomb lattice. The peak at 1715 cm^{-1}, attributes to the C=O stretching vibration of the carboxyl groups. The peaks located at 2930 and 2859 cm^{-1} are ascribed to C-H stretching vibration. The peaks located at 1572, 1218 and 1030 cm^{-1} are ascribed to C=C, C–O (epoxy) and C– O (alkoxy) stretching vibrations, respectively as shown in **Fig. 2a** [**32**].

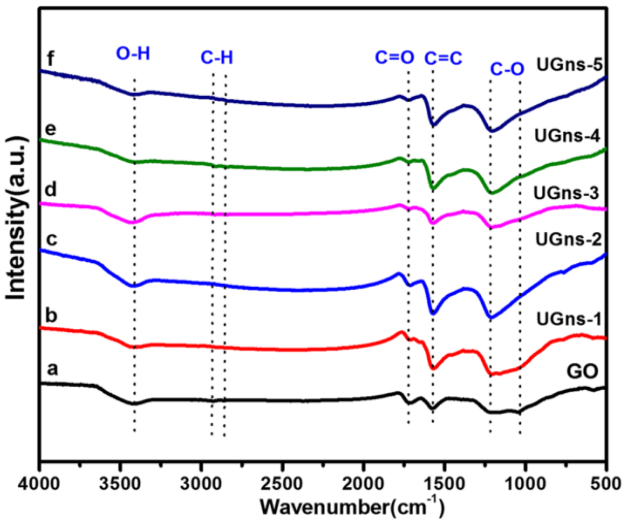

Fig. 2. FTIR spectra of (a) GO, (b) UGns-1, (c) UGns-2, (d) UGns-3, (e) UGns-4 and (f) UGns-5.

After reduction by urea, FTIR spectra of UGns-1 and UGns-2 show suppress bond stretching vibration of C=O (1715 cm^{-1}) and C–O (1030 cm^{-1}), signify that the less removal of oxygen functionalities take place from honeycomb lattice as shown in **Fig. 2b-c**. Meanwhile, FTIR spectrum of UGns-3 shows more suppression in the bond stretching vibration of C=O (1715 cm^{-1}), C–O (1030 cm^{-1}) and O-H (3420 cm^{-1}), which signifies that the more reduction of oxygen functionalities is observed from two dimensional carbon lattice as shown in **Fig. 2d**. In addition, FTIR spectrum of UGns-4 shows the stretching vibrations of C=O (1715 cm^{-1}), C–O (1030 cm^{-1}) and O-H (3420 cm^{-1}) bonds are almost suppressed due to the high removal of oxygen species from carbon skeleton as shown

in **Fig. 2e**. Moreover, FTIR spectrum of UGns-5 shows that the bond starching vibrations at 2859, 1715 and 1030 cm^{-1} are weak; and almost disappears. Additionally, the bond starching vibration of hydroxyl group (O-H) at 3420 cm^{-1} is almost flattened. This strongly indicates that the maximum reduction of oxygen functional groups is observed at 140 °C, which also supports the Raman signature as shown in **Fig. 2f**.

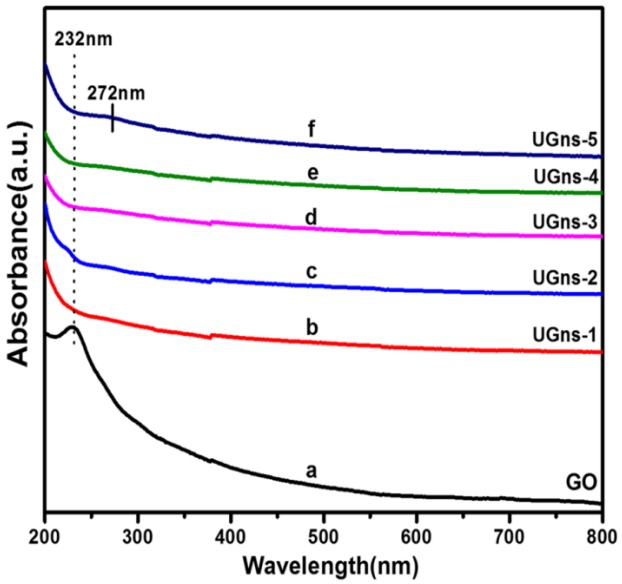

Fig. 3. UV-vis spectra of (a) GO, (b) UGns-1, (c) UGns-2, (d) UGns-3, (e) UGns-4 and (f) UGns-5.

UV–visible spectroscopy (UV-vis)

The characteristic absorbance peaks of GO, UGns-1, UGns-2, UGns-3, UGns-4 and UGns-5 have been analyzed by UV- vis spectroscopy and shown in **Fig. 3**. UV-vis spectrum of GO shows absorption peak at 232 nm, which ascribes to π - $\pi*$ transition of aromatic C–C ring as shown in **Fig. 3a** [**32**]. UV-vis spectra of UGns-1 and UGns-2 show disappearance of GO absorption peak, indicates that the less removal of oxygen species occurs from GO, and layered structure of GO exfoliates into graphene nanosheets as shown in **Fig. 3b-c**. UV-vis spectrum of UGns-3 shows an absorption peak at 266 nm, signifies that the more removal of oxygen functional groups takes place from 2D planner lattice as compared to UGns-1 and UGns-2 as shown in **Fig. 3d**. Whereas, UV-vis spectrum of UGns-4 shows an absorption peak at 268 nm, signifies that the comparatively high removal of oxygen functionalities takes place as shown in **Fig. 3e**. Moreover, UV-vis spectrum of UGns-5 shows well defined absorption peak at 272 nm, which is due to the maximum removal of oxygen functionalities from GO at 140 °C. This confirms the restoration of π-conjugated system due to the change in electronic configuration of graphene nanosheets during reduction process and also validates Raman and FTIR signatures of maximum reduction as shown in **Fig. 3f**.

X-ray diffraction (XRD)

Fig. 4 shows the XRD pattern of graphite powder, GO and UGns-5. **Fig. 4a** shows the XRD pattern of graphite powder, which exhibits a sharp intense peak (002) at 2θ of 26.46° (d ~ 3.35 Å), denotes the crystalline phase of hexagonal graphite. Meanwhile, XRD pattern of GO shows that graphite crystalline peak (2θ of 26.46°) vanishes, which is due to the harsh oxidation of graphite by Hummers method, and new peak arises at 2θ of 12.15° (d ~ 7.23Å). This strongly indicates that the oxygen functionalities have been attached on both side of honeycomb lattice during oxidation of graphite and formation of GO takes place as shown in **Fig. 4b**. XRD pattern of UGns-5 shows that the sharp peak of GO at 2θ of 12.15° (001) disappears after reduction at 140 °C by urea, and reappears a broad peak at 2θ of 24.85° (d ~ 3.57 Å) as shown in **Fig. 4c** [**32**]. This signifies the exfoliation of layered structures of GO into graphene nanosheets and strongly indicates that the π-conjugated system is restored in honeycomb lattice.

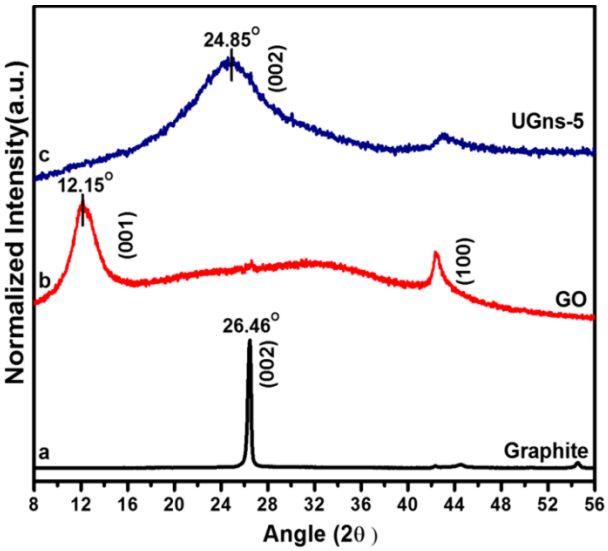

Fig. 4. XRD pattern of (a) graphite, (b) GO and (c) UGns-5.

Field scanning electron microscopy (FESEM)

The surface morphology of the GO and UGns-5 have been investigated by FESEM and shown in **Fig. 5**. FESEM image of GO depicts that the large number of oxygenated graphene flakes are aggregated to each other with lateral sizes ranging from several hundred nanometres to several microns as shown in **Fig. 5a**. After reduction by urea, the GO exfoliates in the individual layers of graphene nanosheets and produces graphene nanosheets. FESEM image of UGns-5 shows the transparent sheet like surface morphology as shown in **Fig. 5b**.

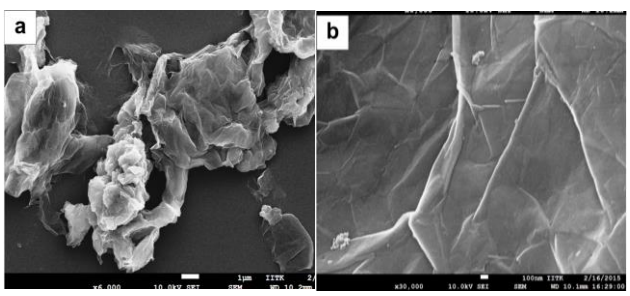

Fig. 5. FESEM image of (a) GO and (b) UGns-5.

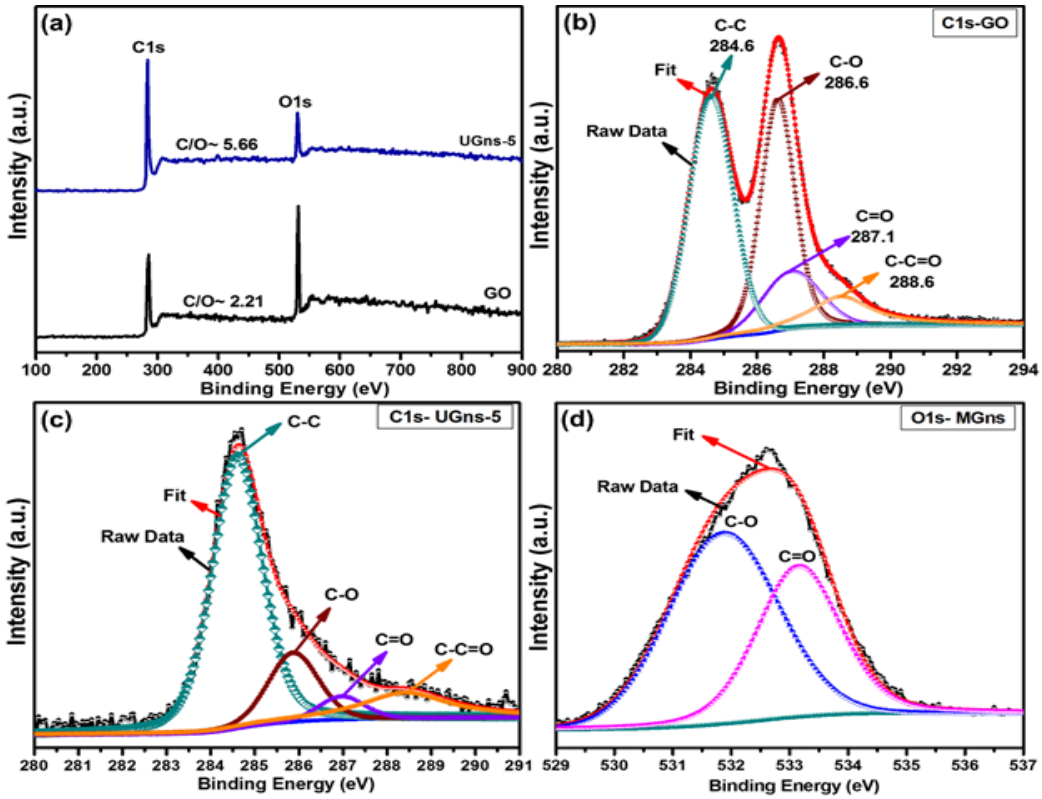

Fig. 6. XPS analysis (a) GO and UGns -5, (b) high resolution spectra C1s of GO, (c) high resolution spectra C1s of UGns-5 and (d) high resolution spectra O1s of UGns-5.

X-Ray photoelectron spectroscopy (XPS)

Surface compositional analysis of the GO and UGns-5 have been carried out by X-ray photoelectron spectroscopy (XPS) as shown in **Fig. 6**. XPS survey spectra of GO and UGns-5 are shown in **Fig. 6a.** XPS survey spectrum of GO confirms the harsh oxidation of graphite by Hummers method. Whereas, XPS survey spectrum of UGns-5 indicates the reduction of GO into graphene nanosheets by green reducing agent, urea. Moreover, the high resolution C1s spectrum of GO fitted with Shirley background ascribes two sharp intense peaks corresponding to C-C and C-O bonds of carbon atoms in 2D planner lattice with binding energies of 284.6 and 286.6 eV, respectively. In addition, carbon bonding configurations with binding energies of 287.1 and 288.6 eV are attributed to C=O and C-C=O bonds present in the honeycomb lattice, indicates the rasping oxidation and destruction of the sp^2 atomic structure of graphite as shown in **Fig. 6b** [**33**]. Meanwhile, the substantial decrease in the oxygen related peaks intensities has been observed in the high resolution spectrum of C1s of UGns-5 as compared to GO after reduction by urea at 140 °C; and C/O ratio increases from 2.21 to 5.66, strongly indicates that the π-delocalized conjugation is restored in the carbon skeleton as shown in **Fig. 6c**. Furthermore, high resolution spectrum of O1s of UGns-5 is shown in **Fig. 6d**. The spectrum of O_2 consists of two peaks at 532.1 and 533.2 eV, which can be assigned to C-O and C=O respectively. Hence, XPS indicates that the urea offers excellent reductive ability at 140 °C to produce graphene nanosheets. The comparison of I_D/I_G and C/O ratio reported by different reducing agents with processing temperature [**34-39**] has been tabulated in **Table 1** and confirms that the urea offers excellent reductive ability at high temperature for the removal of oxygen functional groups from GO.

Table 1. Reduction of GO using different reducing agents.

Reducing agent	T (°C)	I_D/I_G	C/O	Reducing agent issue	Ref.
N_2H_4	180	1.56	7.00	Toxic	**[34]**
$NaHSO_3$	95	1.22	2.23	Harmful	**[35]**
N_2H_4	95	1.15	15.1	Toxic	**[36]**
N_2H_4	50	1.77	5.40	Toxic	**[37]**
Na_3PO_2	90	1.39	13.5	Harmful	**[38]**
$NaBH_4$	27	1.70	8.60	Hazardous	**[39]**
CH_4N_2O	140	1.41	5.66	Green	Present work

Conclusion

In summary, temperature dependant study on the reductive ability has been demonstrated for GO via solution-processable method using green reducing agent, urea. The reductive ability of urea has been tested over a range of temperature i.e., 27 to 140 °C. Raman analysis confirms that the degree of reduction increases when temperature is raised from 90 to 140 °C. Maximum removal of oxygen functional groups is observed at 140 °C, and reached to I_D/I_G ratio of ~ 1.41. FTIR analysis validates the Raman signature of removal of oxygen functional groups from GO at 140 °C. Further, elemental analysis has been carried out to test the surface composition, which also confirms the successful removal of oxygen species from GO, and attainment of the C/O ratio of ~ 5.66. These results signify that the urea offers

excellent reductive ability at high temperature for the removal of oxygen functional groups from GO.

Acknowledgements

The authors acknowledge the financial support provided by the Indian Institute of Technology Kanpur, India for carrying out this research work.

References

1. Novoselov, K.S.; Falko, V.I.; Colombo, L.; Gellert, P.R.; Schwab, M.G., Kim, K; *Nature*, **2012**, *490*, 192. **DOI:** 10.1038/nature11458
2. Tiwari, A.; Syvajarvi, M. (Eds.); Graphene Materials: Fundamentals and Emerging Applications; Wiley: USA, **2015**. **DOI:** 10.1002/9781119131816
3. Mishra, A. K.; Ramaprabhu, S; *J. Appl. Phys.*, **2014**, *116*, 064306. **DOI:** 10.1063/1.4892458
4. Chamoli, P.; Das, M.K.; Kar, K.K.; *Graphene*, **2015**, *3*, 56. **DOI:** 10.1166/graph.2015.1060
5. Kar, K.K.; Pandey, J.K.; Rana, S.K. (Eds.); Handbook of Polymer Nanocomposites. Processing, Performance and Application, Volume B: Carbon Nanotube Based Polymer Nanocomposites; Springer Heidelberg New York Dordrecht: London, **2015**. **DOI:** 10.1007/978-3-642-45229-1
6. Tiwari, A.; Shukla, S.K. (Eds.); Advanced Carbon Materials and Technology; Wiley: USA, **2013**. **DOI:** 10.1002/9781118895399
7. Patra, S.; Roya, E.; Tiwari, A.; Madhuri, R.; Sharma, P. K; *Biosens. Bioelectron.*, **2016**. **DOI:** 10.1016/j.bios.2016.02.067
8. Gautam, R; Banerjee, S.; Kar, K.K; *Recent Pat. Mater. Sci.*, **2015**, *8*, 15. **DOI:** 10.2174/1874464808666150306223104
9. King, A.A.K.; Davies, B.R.; Noorbehesht, N.; Newman, P.; Church, T.L.; Harris, A.T.; Razal, J.M.; Minett, A.I; *Sci. Rep.*, **2016**, *6*, 19491. **DOI:** 10.1038/srep19491
10. A. Tiwari, M. Syväjärvi (Eds), In Advanced 2D Materials, John Wiley & Sons, Beverly, MA, USA, **2016**.
11. Hayes, W.I.; Joseph, P.; Mughal, M.Z.; Papakonstantinou, P; *J. Solid State Electrochem.*, **2015**, *19*, 361. **DOI:** 10.1007/s10008-014-2560-6
12. Liu, C.; Hao, F.; Zhao, X.; Zhao, Q.; Luo, S.; Lin, H; *Sci. Rep.*, **2014**, *4*, 3965. **DOI:** 10.1038/srep03965
13. Hu, Z.T.; Liu, J.; Yan, X.; Oh, W.D.; Lim, T.T; *Chem. Eng. J.*, **2015**, *262*, 1022. **DOI:**10.1016/j.cej.2014.10.037
14. Williams, G.; Seger, B.; Kamat, P.V; *ACS Nano*, **2008**, *2(7)*, 1487. **DOI:** 10.1021/nn800251f
15. Feng, Y.; Feng, N.; Du, G.; *RSC Adv.*, **2013**, *3*, 21466. **DOI:** 10.1039/C3RA43025A
16. Akhavan, O.; Kalaee, M.; Alavi, Z.S.; Ghiasi, S.M.A.; Esfandiar, A; *Carbon*, **2012**, *50*, 3015. **DOI:**10.1016/j.carbon.2012.02.087
17. Fernández-Merino, M.J.; Guardia, L., Paredes, J.I., Villar-Rodil, S.; Solís-Fernández, P.; Martínez-Alonso, A.; Tascón, J.M.D; *J. Phys. Chem. C*, **2010**, *114*, 6426. **DOI:** 10.1021/jp100603h
18. Akhavan, O.; Ghaderi, E.; Aghayee, S.; Fereydooni, Y.; Talebia, A.; *J. Mater. Chem.*, **2012**, *22*, 13773. **DOI:** 10.1039/C2JM31396K
19. Zhu, C.; Guo, S.; Fang, Y.; Dong, S; *ACS Nano*, **2010**, *4*, 2429. **DOI:** 10.1021/nn1002387
20. Esfandiar, A.; Akhavan, O.; Irajizad, A; *J. Mater. Chem.*, **2011**, *21*, 10907. **DOI:** 10.1039/C1JM10151J
21. Liu, J.; Fu, S.; Yuan, B.; Li, Y.; Deng, Z; *J. Am. Chem. Soc.*, **2010**, *132*, 7279. **DOI:** 10.1021/ja100938r
22. Akhavan, O.; Ghaderi, E.; Abouei, E.; Hatamie, S.; Ghasemi, E; *Carbon*, **2014**, *66*, 395. **DOI:**10.1016/j.carbon.2013.09.015
23. Akhavan, O.; Ghaderi, E; *Carbon*, **2012**, *50*, 1853. **DOI:**10.1016/j.carbon.2011.12.035
24. Hatamie, S.; Akhavan, O.; Sadrnezhaad, S.K.; Ahadian, M.M.; Shirolkar, M.M.; Wang, H.Q; *Mater. Sci. Eng. C*, **2015**, *55*, 482. **DOI:**10.1016/j.msec.2015.05.077
25. Akhavan, O; *Carbon*, **2015**, *81*, 158. **DOI:**10.1016/j.carbon.2014.09.044
26. Chamoli, P.; Das, M. K.; Kar, K. K; *Curr. Nanomater.*, **2016**, *1*, 110. **DOI:**.10.2174/2468187306666160624113837
27. Lei, Z.; Lu, L.; Zhao X.S; *Energy Environ. Sci.*, **2012**, *5*, 6391. **DOI:** 10.1039/C1EE02478G
28. Yang, Y.; Wang, H.; Wang, L.; Ge, Y.; Kan, K.; Shi, K.; Chen, J; *New J. Chem.*, **2016**, *40*, 4678. **DOI:** 10.1039/C5NJ03284A
29. Sharon, M.; Sharon, M.; Shinohara, H.; Tiwari, A. (Eds.); Graphene: An Introduction to the Fundamentals and Industrial Applications; Wiley: USA, **2015**. **DOI:** 10.1002/9781118842577
30. Ferrari, A.C.; Basko, D.M; *Nat. Nanotechnol.*, **2013**, *8*, 235. **DOI:** 10.1038/nnano.2013.46
31. Lee, B. S.; Lee, Y.; Hwang, J. Y.; Choi, Y. C; *Carbon Letters*, **2015**, *16(4)*, 255. **DOI:** 10.5714/CL.2015.16.4.255
32. Yang, S.; Yue, W.; Huang, D.; Chen, C; Lin, H.; Yang, X; *RSC Adv.*, **2012**, *2*, 8827. **DOI:** 10.1039/C2RA20746J
33. Some, S.; Kim, Y.; Yoon, Y.; Yoo, H.J.; Lee, S.; Park, Y.; Lee, H.; *Sci. Rep.*, **2013**, *3*, 1929. **DOI:** 10.1038/srep01929
34. Wang, R.; Wang, Y.; Xu, C; Sun, J.; Gao, L; *RSC Adv.*, **2013**, *3*, 1194. **DOI:** 10.1039/C2RA21825A
35. Chen, W.; Yan, L.; Bangal, P. R; *J. Phys. Chem. C* **2010**, *114*, 19885. **DOI:** 10.1021/jp107131v
36. Ren, P.G.; Yan, D.X.; Ji, X.; Chen, T.; Li, Z.M; *Nanotechnology*, **2010**, *22*, 055705. **DOI:** 10.1088/0957-4484/22/5/055705
37. Lee, K. H.; Lee, B.; Hwang, S. J.; Lee, J. U.; Cheong, H., Kwon, O.S.; Shin, K.; Hur, N. H; *Carbon*, **2014**, *69*, 327. **DOI:** 10.1016/j.carbon.2013.12.031
38. Wang, Xin; Xing, W.; Yu, B.; Feng, X.; Song, L.; Hu, Y. *J. Mater. Chem. C*, **2013**, 1, 690. **DOI:** 10.1039/C2TC00259K
39. Shin, H. J.; Kim, K. K.; Benayad, A.; Yoon, S. M.; Park, H. K.; Jung, I.S.; Jin, M. H.; Jeong, H. K.; Kim, J. M.; Choi, J.Y.; Lee, Y. H; *Adv. Funct. Mater.*, **2009**, *19*, 1987. **DOI:** 10.1002/adfm.200900167